Chin. J. Astron. Astrophys. Vol. 6 (2006), No. 5, 617–624
(*http://www.chjaa.org*)

Chinese Journal of
Astronomy and
Astrophysics

Derivation of the Spiral Motion of an Eruptive Prominence and Its Explanation

Xiao-Ma Gu[1], Shu-Hua Zhong[1], Hong-Fei Liang[1] and La-Sheng Zhan[2]

[1] National Astronomical Observatories / Yunnan Observatory, Chinese Academy of Sciences, Kunming 650011; *xmgu@ynao.ac.cn*
[2] Jingdezhen Ceramic Institute, Jingdezhen 333000

Received 2006 January 26; accepted 2006 April 21

Abstract A 2D velocity field of the eruptive prominence (EP) of 1991 March 5 is obtained from its spectral data observed at the Yunnan Observatory and the velocity distributions along the entrance slit are derived for different observing frames. Under the assumption that matter in the EP undergoes axial, radial and possible rotational motions, we construct a theoretical velocity distribution of the EP along the entrance slit, to derive, by fitting, the angular velocity of rotation ω and the other three parameters (axial velocity v_0, radial velocity v_r and the angle between the EP plane and the line of sight ϕ). We found: an averaged angular velocity ω of 3.0×10^{-3} arc s^{-1} and the variation of ω with the height above the solar limb. As the EP rises, the matter within it in fact moves along a spiral path around its axis. The spiral motion may be explained by the theory of plasma 'double pole diffusion' (DPD) caused by a sharp density gradient between the eruptive prominence and the surrounding corona. A theoretical angular velocity ω' is estimated based on the DPD and basically coincides with ω obtained from the optimal velocity fitting.

Key words: Sun: eruptive prominence — Sun: Spiral motion

1 INTRODUCTION

Prominence eruption is an important phenomenon of solar activity and has been studied for several decades. In recent times, it is found that prominences and their eruptions have a close connection with the coronal mass ejection (CME), arousing further interest in their study (Schmieder et al. 1997; Wood et al. 1999; Plunkett et al. 2000) with emphases on the following questions: Why does prominence erupt? What is the mechanism of the eruption? How to explain the kinematic characters of the eruptive prominences?

Several models of CMEs including eruptive prominence (EP) were put forward by different authors (Chen 1996; Antiochos et al. 1999; Lin et al. 1998; Forbes 2000; Klimchuck 2001; Low 2001; Priest & Forbes 2002; Lin et al. 1995, 2002, 2003; Lin 2002) and a well-written review on the theories of solar eruptions was given by Lin et al. (2003).

Simultaneous SOHO and ground-based observations of a large EP and CME were presented by Plunkett et al. (2000). The prominence was found to rotate about its axis as it moved outward and the CME contained a helical structure consistent with an ejection of a magnetic flux rope from the Sun. Karlický & Šimberová (2002) observed a vertical coil-like (helical) structure for the eruptive prominence of 2000 March 20.

On 1991 March 5, a large EP occurred on the solar eastern limb. It was observed with a two-dimensional multi-waveband spectra-spectroheliograph (MW-SSHG) at the Yunnan Observatory (Xuan & Lin 1993). The 2D H$_\alpha$ spectral data of the prominence were analyzed quantitatively, and the 2D distributions of four physical quantities (N_2, $T_{\rm ex}$, $V_{\|}$ and V_t) and their physical structure were given by Zhong et al. (2004, hereafter 'Paper I'). In the present paper, we will further study the line-of-sight velocity field, derive its spiral motion and provide a possible explanation for the helical motion of the material within the EP.

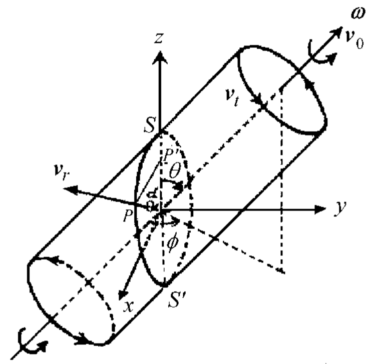

Fig. 1 Sketch of the right-handed system at the position of the eruptive prominence. Here V_0, V_r and V_t are the velocity components in the axial, radial and tangential directions, respectively.

2 KINEMATIC MODEL OF THE ERUPTIVE PROMINENCE

Observations, data reduction and analysis of the eruptive prominence were described in detail by Zhong et al. (Paper I), and details of the method were also given by Gu et al. (2001, 2002).

2.1 Movement of the Eruptive Prominence

We suppose that the eruptive prominence (EP) is in the shape of a cylinder and in general the matter within the EP is in three motion modes: along the axial and radial directions, and rotation around its axis; expansion and contraction are included in the radial motion. Let us setup a right-handed Cartesian coordinate system $(O - xyz)$ as shown in Figure 1, with origin O is on the column axis, the z-axis along the entrance slit and the x-axis pointing to the observer. In this system, let θ be the angle of the column axis measured from the z-axis, ϕ, the angle of the projection of the column axis on the xOy plane measured from the x-axis. Generally, this system can move along the line-of-sight with speed V_{cs}; a positive sign denotes motion away from the observer. In this case, the EP plasma near its edge can move axially with speed $\boldsymbol{V}_0$, radially with speed $\boldsymbol{V}'_r$ and tangentially with speed $\boldsymbol{V}'_t$. Thus we have

$$\begin{aligned}
\boldsymbol{V}_0 &\equiv (v_0 \sin\theta\cos\phi, v_0 \sin\theta \sin\phi, v_0 \cos\theta),\\
\boldsymbol{V}_r &\equiv (v'_r \cos\theta\cos\phi, v'_r \cos\theta\sin\phi, v'_r \sin\theta),\\
\boldsymbol{V}_t &\equiv (-v'_t \cos\theta\sin\phi, v'_t \cos\theta\cos\phi, v'_t \sin\theta),\\
\boldsymbol{V}_{cs} &\equiv (v_{cs}, 0, 0).
\end{aligned}$$

So, the total velocity of the EP in the $-x$ direction is

$$V_{\|} = -(v_0 \sin\theta\cos\phi + v'_r \cos\theta\cos\phi - v'_t \cos\theta\sin\phi) + v_{cs}, \tag{1}$$

where the sign (–) is added for positive Doppler velocities away from the observer. In order to compare with the velocities derived from spectral observation, it is necessary to rewrite the form of Equation (1). Considering v'_r and v'_t are related to the positions on the surface of the EP, we derive different velocities from the spectral data at different sites of the slit (where the EP intersects with it). For simplicity, we suppose that the coordinate system does not move along the line-of-sight, so $v_{cs} = 0$. In Figure 1, the elliptical section represents the intersection between the EP column and the x-z coordinate plane, P is an arbitrary point on the surface of the EP, which corresponds to the j^{th} measured point P' on the slit and to a position angle of α on the arc of SP (in Fig. 1, $\geq$0 and $\leq 180°$), so, $v'_r = v_r \sin\alpha$, $v'_t = v_t \cos\alpha$, v'_r and v'_t are the respective X-components of the radial and tangential velocities at the site of p. Thus, we have

$$V_{\|} = -(v_0 \sin\theta\cos\phi + v_r \cos\theta\cos\phi\sin\alpha - v_t \cos\theta\sin\phi\cos\alpha). \tag{2}$$

2.2 Fitting of the Velocities

To compare the theoretical and observed velocities, we assume there are m measured points along the entrance slit in the frame (see Fig. 1), $SS' = m$, P' is the j^{th} measured point, and if the angle α is expressed with the number of the measured point, m, then

$$\cos\alpha \cong 1 - \frac{2(j-1)}{m-1}\,, \tag{3}$$

where, $j = 1, 2, 3, \ldots m$ (for $j = 1$ and m, $\alpha = 0$ and $180°$, respectively). On the other hand, $v_t = \omega R$, R is the radius of the EP at the p site, ω is the rotational angular velocity of the EP at the same point. If $Z_{\max}$ denotes the maximum of the EP on the z-axis, then the correlation between R and $Z_{\max}$ is

$$R = \frac{\sin\theta\sin\phi}{\sqrt{1-\sin^2\theta\cos^2\phi}} Z_{\max}. \tag{4}$$

It is expected when $\theta = \phi = 90°$, then $R = Z_{\max}$, consistent with Equation (4). Considering one half of the entrance slit that intersects with the EP, $Z_{\max}$ (i.e., OS in Fig. 1) is different for the different spectral frames. In terms of m, we have $Z_{\max} = d(m-1)/2$, d being the distance between two adjacent measured points ($d = 2.4 \times 10^3$ km). So,

$$v_t = \frac{m-1}{2}\frac{\omega d\sin\theta\sin\phi}{\sqrt{1-\sin^2\theta\cos^2\phi}}. \tag{5}$$

Here two relations will be used, namely, $\cos\theta = \pm 1/\sqrt{1+\tan^2\theta}$ and $\sin\theta = \pm\tan\theta/\sqrt{1+\tan^2\theta}$. On the other hand, we have (see Fig. 2)

$$\tan\theta = \frac{\tan\beta}{\sin\phi}. \tag{6}$$

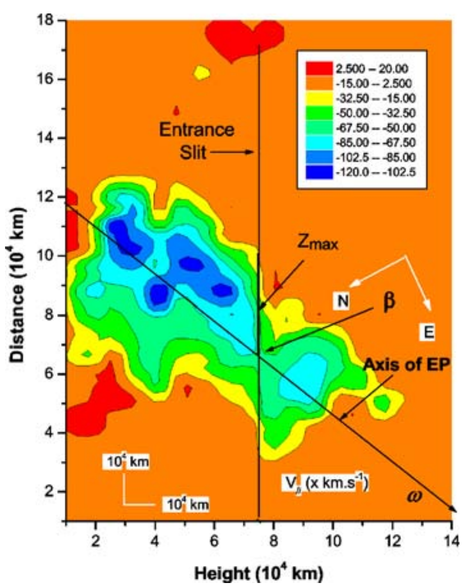

Fig. 2 2D line-of-sight velocity field of the EP taken during 03:30–03:33 UT, in units of km s^{-1}, β is the angle between the entrance slit and the projection of the EP axis on the heaven plane, ω is the rotational angular velocity around the axis of the EP.

Table 1 Values of v_0, v_r, ϕ, and ω in the Different Frames

Frame	m	$-v_0$ (km s^{-1})	$-v_r$ (km s^{-1})	ϕ (deg)	ω (10^{-3} arc s^{-1})	Error
13	23	68.66	187.12	14.91	2.160	4.091
14	23	70.16	182.62	14.89	2.155	4.138
15	23	79.74	179.89	14.80	3.499	4.542
16	22	43.58	263.52	14.84	2.384	3.143
17	21	85.61	171.33	14.67	1.042	1.404
18	17	66.94	142.14	15.47	11.440	0.508
19	17	68.27	79.61	15.11	7.085	0.527
20	16	56.97	40.07	15.08	4.910	0.328
21	16	82.89	60.50	14.94	1.481	0.679
22	17	105.50	144.12	14.59	–2.296	0.883
23	14	64.94	92.61	15.36	–3.696	0.787
24	12	54.27	91.69	15.16	3.271	1.043
25	11	67.86	77.09	14.93	5.892	0.987

Note: Negative v_0 and v_r values mean velocities towards the observer. Average values of ϕ =15° and ω=3.0 × 10^{-3} arc s^{-1}.

Here, β can be measured directly on the H$_\alpha$ filtergram of 03:33 UT (figure 1 in Paper I), $\beta \approx 120.5°$. Therefore, we have

$$V_{\|} = -\Big[v_0 \sin\theta\cos\phi + v_r \cos\theta\cos\phi\sin\alpha - \frac{(m-1)}{4}\frac{d\omega\sin 2\theta\cos\alpha\sin^2\phi}{\sqrt{1-\sin^2\theta\cos^2\phi}}\Big]. \tag{7}$$

If we take $V_{\|}^{\rm theo}(j, v_0, v_r, \phi, \omega) \equiv V_{\|}(j)$ and $V_{\|}^{\rm obs}(j)$ referring to the $j^{\rm th}$ velocity derived from the spectral observation of a spectral frame, where v_0, v_r, ϕ, ω are the parameters to be determined. In this case, the best representation of the observed velocity $V_{\|}^{\rm obs}\,(j)$ is obtained when

$$\Psi(v_0, v_r, \phi, \omega) = \sum_{j=1}^{m}[V_{\|}^{\rm theo}(j) - V_{\|}^{\rm obs}(j)]^2 \tag{8}$$

is a minimum. We use a simplex method (Li & Ding 1992; Li et al. 1993, 1995) to make the objective function Ψ to be a minimum, thus, the four parameters (v_0, v_r, ϕ, ω) are derived simultaneously by the optimal fitting between the theoretical velocity $V_{\|}^{\rm theo}$ and the observed one, $V_{\|}^{\rm obs}$. We made the fitting for 13 spectral frames (frame numbers 13 to 25) and the results are listed in Table 1. It will be shown that the velocity distribution derived from spectral observation for each frame is multi-smoothed, because the velocities have a larger dispersion along the entrance slit. The distributions of the line-of-sight velocity along the entrance slit are given in Figure 3. In the figure circular and square points indicate respectively the theoretical and observed velocities. Figure 3 shows the fittings are basically acceptable; the error of fitting is smaller for the higher spectral frames than that for the lower ones (ref. column 7 in Table 1). The high velocity "mound" structures (see the blue and dark blue areas in Fig. 2) in the lower spectral frames (near the solar limb) make the velocity depart from the theoretical model.

2.3 Height Variation of ω, v_0 and v_r

Figure 4 shows the variation with the height, within a short time (say, a few minutes), of the rotational angular velocity ω, and the axial and radial velocities v_0, v_r. It is found that ω seems to show a periodic, sine-like, variation with the height, a reflection of spiral motion. From frames 5 to 12, we can estimate the increase of height after each full rotation (which takes about 35 minutes) to be about 2.8 $\times 10^{4}$ km, hence we derive an ascending velocity of about 13.4 km s^{-1}. In addition, v_r decreases with the height, but there were two increments in v_r, one of 84 km s^{-1} at heights 2.0×10^4 km (frame 15) and one of 74 km s^{-1} at height 4.4×10^4 km (frame 21). There was no evident height variation in v_0 above the solar limb.

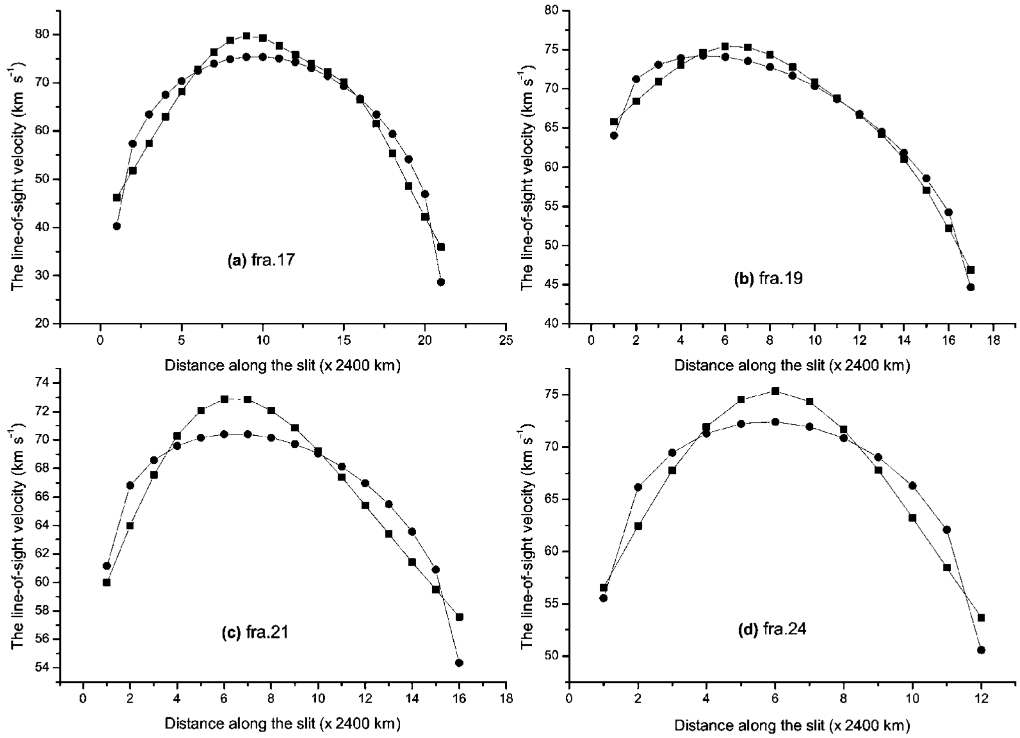

Fig. 3 Distribution of the line-of-sight velocity along the entrance slit. Circles refer to the theoretical velocities, squares, velocities derived from spectral observation. Different observing frames correspond to different heights above the solar limb; (a), (b), (c) and (d) correspond to frames 17, 19, 21, and 24, respectively. The left side of the figures corresponds to the top of the EP in Fig. 2.

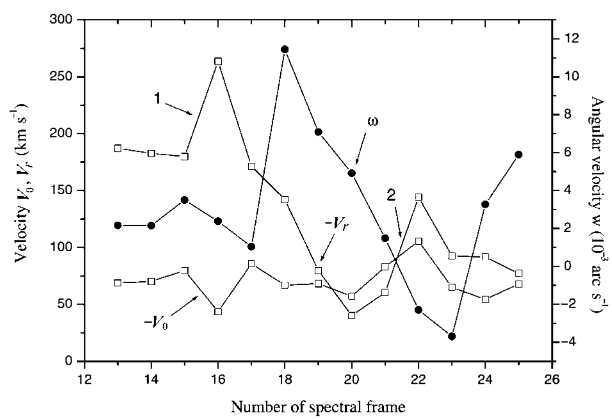

Fig. 4 Variation of the axial velocity V_0, radial velocity V_r and angular velocity ω across the different observed frames, $5.5''$ ($\approx 4 \times 10^3$ km in height) apart.

3 EXPLANATION OF THE HELICAL MOTION

A helical movement of the EP has been obtained during its rise, the question is why, or what mechanism makes it rotate? Xu et al. (1984) proposed a mechanism of 'double pole diffusion' (DPD) of plasma which successfully explained the helical motion of the surge of 1980 October 11. Li (1995) also applied the DPD mechanism to the surge of 1989 March 19. Here, we will consider whether the DPD mechanism is valid for the eruptive prominence of 1991 March 5.

We understand that the existence of a sharp density gradient between the plasma of eruptive prominence and that of the surrounding corona will cause an induced electric field. Because magnetic field is frozen in the EP material, this electric field will give rise to an electric drift of the plasma material near the limb of the EP, the interaction force between the magnetic field within the EP and the electric field, $\boldsymbol{E} \times \boldsymbol{B}$, is in the tangential direction of the EP column and it will make the EP material near the limb rotate (see Fig. 5). The electric field caused by the DPD in plasma is given by

$$\boldsymbol{E} = -\frac{|e|(D_e - D_i)}{\sigma_e - \sigma_i} \nabla_r N \,, \tag{9}$$

where D_e and D_i are the diffusion efficiencies of electrons and ions, σ_e and σ_i are the corresponding conductivities. Considering $\sigma_e \gg \sigma_i$ and $D_e \gg D_i$, we can express $\boldsymbol{E}$ as

$$\boldsymbol{E} = -\frac{|e| D_e}{\sigma_e} \nabla_r N \,, \tag{10}$$

where D_e and σ_e are approximately $kT_e\tau_e/m_e$ and $e^2N_e\tau_e/m_e$, respectively. Now the ejection features of the EP look like a surge, so we consider that the EP materials may come from a region where the electrical conductivity σ_e^* is abnormal, and we have, according to Bunemann's results (Heyvaerts et al. 1977), $\sigma_e^* = 10^{-5}\sigma_e$, thus Equation (10) becomes

$$\boldsymbol{E} = -10^5 \frac{|e| D_e}{\sigma_e} \nabla_r N \,. \tag{11}$$

The drift velocity, namely the linear velocity of rotation, due to electric field $\boldsymbol{E}$, is

$$\boldsymbol{V}_t = \frac{c}{B^2} (\boldsymbol{E} \times \boldsymbol{B}). \tag{12}$$

Combine Equations (11) and (12), we have

$$V_t = 10^5 \frac{ckT}{eB} \frac{|\nabla_r N|}{N}, \tag{13}$$

where $V_t = \omega' R$, ω' is the theoretical rotational angular velocity and R the radius of the EP column, so,

$$V_t = \frac{\omega' \sin\theta \sin\phi}{\sqrt{1 - \sin^2\theta \cos^2\phi}} Z_{\max}, \tag{14}$$

Substitute Equation (14) into Equation (13), we obtain

$$\frac{\omega' \sin\theta \sin\phi}{\sqrt{1 - \sin^2\theta \cos^2\phi}} Z_{\max} = 10^5 \frac{ckT}{eB} \frac{|\nabla_r N|}{N} \,. \tag{15}$$

Considering the average value of ϕ is 14.8°, from Equation (6), we have $\theta \approx 98.6°$ and we obtain, after simplification,

$$\omega' = 0.10 \times 10^{10} \frac{T}{Z_{\max} B} \frac{|\nabla_r N|}{N} \,, \tag{16}$$

where $Z_{\max} = (2.6 - 0.48) \times 10^4$ km (corresponding to frames 13–25), as determined directly from the spectral images; the temperature equals 1.8×10^4 K on average (see fig. 4 of Paper I). Raadu et al. (1987) studied a material ejection on 1981 June 22 and gave a magnetic field B between 10 G and 30 G, so we take $B = 15$ G. From the specific parameter values of the EP of 1991 March 5, we estimate the depth of the EP boundary to be $8 \sim 30$ km, i.e. $\frac{N}{|\nabla_r N|} = (8 \sim 30)$ km, so, the rotational angular velocity estimated theoretically from Equation (16), ω', is between 0.12 and 3.13×10^{-3} arc s^{-1}; it is about 1.63×10^{-3} arc s^{-1} on average (it takes about 64 minutes to make a full rotation), the variation range of ω' is almost same as that of ω, the directions of ω and ω' are the same and point to the top of the EP. The result estimated based on the mechanism of DPD is basically accordant with that obtained from the velocity fitting (see Table 1). Thus, the mechanism of plasma DPD enables us to explain successfully the helical motion of the EP during its rise.

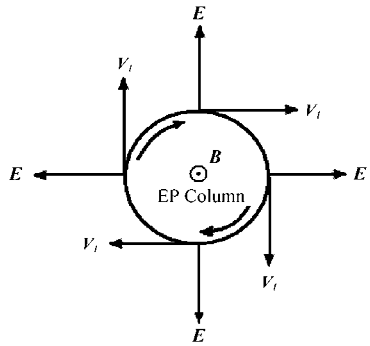

Fig. 5 Schematic of rotational motion produced by the plasma DPD effect caused by a sharp density gradient between the EP and the surrounding corona. $\boldsymbol{B}$ is magnetic field towards the observer and the arrow within the EP indicates the direction of material movement.

4 DISCUSSION

It should be pointed out that the observed H_α radiation mainly comes from the surface layer of the EP, because the H_α line is optically thick and any radiation from the deeper layers will not reach the observer. Thus, the velocity derived from H_α spectral data is an average value over the observed part of the surface layer of the EP. Considering the measuring errors and the low temporal resolution of the observation, the total error in the velocities is estimated to be within ± 5 km s^{-1}. Many EUV observations show that eruptive prominence usually exhibits structural inhomogeneity, so, in some cases the region we can actually see is on the opposite layer of the EP, then the rotation obtained may be different. If this is the case then our method may be questionable. To avoid this difficulty, we suppose, as a simplification and approximation, that the material within the EP fills the layer facing the observer, so that we need not heed any structural inhomogeneity within the EP. On the other hand, the axial, radial and tangential velocities derived from our model are belong to the EP surface facing the observer; owing to the sharp density gradient between the EP and the surrounding corona, the velocity computed with the DPD theory is also on the surface layer facing the observer, thus, the three velocities (computed and derived from the model and observation) all refer to the same layer of the EP and are thus comparable.

As the EP rises, the pressure difference between the EP and the surrounding corona increases. When it exceeds a critical value then an explosive expansion takes place. However, the expansion is not continuous, because after the first expansion it requires certain time to reach a new critical value of the pressure difference. Within the same time interval, different expansions happen at different heights (ref. 1 and 2 of V_r in Fig. 4).

It can be found from Figure 4 that the radial velocity V_r has two leaps (labelled 1 and 2 in Fig. 4), one in height range (2.0–2.4)$\times 10^4$ km and one in (8.4–8.8)$\times 10^4$ km. A large leap in V_r means an explosive expansion taking place in the EP. Because the pressure in the corona decreases with the height, the pressure difference between the EP and the surrounding corona is decreased with the height (after each expansion), thus, successive expansions get weaker and weaker: the two expanding velocities were about 84 and 74 km s^{-1}, respectively.

There is a close relation between the radial velocity V_r and the angular velocity ω. When V_r suddenly increases, it means that an explosive expansion has taken place, at that time ω will decrease (compare the curves V_r and ω in Fig. 4), because V_r includes the expansion velocity, the density within the EP decreases when it expands, the density gradient between the EP and the surrounding corona also decreases. Therefore, it makes the effect of plasma DPD weaker and the rotation velocity smaller. It also indicates that the obtained results of fitting theoretical and observational velocities are reliable.

Table 1 and Figure 4 show that ω undergoes a cyclical change with height, which is a reflection of helical motion, and which may also be caused by changes in T, B and $Z_{\max}$. In fact, T, B and $Z_{\max}$ are mutually constrained. Thus, the computed value from Equation (16) gives an alternative range of $\omega\,'$. The good agreement between the theoretical estimation and those obtained from the optimal fitting of the theoretical and observed velocities indicates that the mechanism of plasma DPD is valid for explaining the helical movement of EPs. In general, the conditions for DPD of plasma are satisfied in the solar atmosphere, that is why some helical movements are usually observed in eruptive events such as surges, EPs, CMEs, etc.

5 CONCLUSIONS

A spiral motion of the eruptive prominence of 1991 March 5 is derived and investigated based on the 2D spectral data obtained at the Yunnan Observatory. We constructed a theoretical model of material motion within the EP, and then made an optimal velocity fitting between the theoretical velocity distribution along the entrance slit and the observed one derived from the 2D spectral data. We obtained a rotational motion with an average angular velocity $\boldsymbol{\omega}$ of 3.0×10^{-3} arc s^{-1} during the rise, thus showing that the eruptive prominence actually was in a helical motion along its axial direction. The value of $\boldsymbol{\omega}$ changed by about $(1.0 \sim 5.0) \times 10^{-3}$ arc s^{-1}, exhibited a cycle variation relative to the height above the solar limb, and took about 35 minutes to complete a rotation. The direction of $\boldsymbol{\omega}$ coincides with that of the rise of the eruptive prominence. We also found the expansion effect of the EP in different heights at the same moment, the explosion-like expansions are not continuous and the expanding velocity decreases with increasing height.

We estimate the drift velocity V_t produced by an electric field $\boldsymbol{E}$ caused by the DPD of plasma formed by a sharp density gradient between the eruptive prominence and the surrounding corona. Both magnitude and direction of the angular velocity computed based on the theory of plasma DPD are basically accordant with that of the angular velocity derived from the spectral observations. The helical motion of the eruptive prominence can be explained by the theory of the plasma DPD. Such helical motion may be a general characteristic of material motion in all mass ejections in the solar atmosphere (where the conditions for the DPD of plasma are usually satisfied), including surges, CMEs, EPs, etc. Of course, we need more studies to prove this thesis.

Acknowledgements The authors thank Profs. Jun Lin and Ke-Jun Li for providing kind supports for the work. We are grateful to the anonymous referee for giving very helpful comments on the manuscript. We would like to thank Ms. Hui-Bo Shen, one of the PDS staff at the Purple Mountain Observatory, CAS, for helping with the digitization of the spectral data.

References

Antiochos S. K., DoVore C. R., Klimchuk J. A., 1999, ApJ, 510, 485
Chen J., 1996, J. Geophys. Res., 101, 27499
Forbes T. G., 2000, J. Geophys. Res., 105, 23153
Gu X. M., Dun J. P., Zhong S. H., 2001, A&A, 380, 704
Gu X. M., Ding M. D., 2002, Chin. J. Astron. Astrophys. (ChJAA), 2, 92
Heyvaerts J., Priest E. R., Rust D. M., 1977, ApJ, 216, 123
Klimchuk J. A., 2001, In: Song P., Singer H. eds., Space Weather, AGU Monograph 125, p.143
Karlický M., Šimberová S., 2002, A&A, 388, 1016
Li K. J., Ding Y. J., 1992, Acta Astron. Sin., 33, 171
Li K. J., Ding Y. J., Bei J. M. et al., 1993, AJ, 106, 396
Li K. J., Ding Y. J., Zhong S. H., 1995, MNRAS, 274, 689
Li K. J., 1995, Proc. of the China-Japan Seminar on Solar Physics, International Academic Publishers, Beijing, p.83
Lin J., 2002, Chin. J. Astron. Astrophys. (ChJAA), 2, 539
Lin J., Forbes T. G., Isenberg P. A. et al. , 1998, ApJ, 504, 1006
Lin J., Forbes T. G., Priest E. R. et al., 1995, SoPh, 159, 275
Lin J., van Ballegooijen A. A., Forbes T. G., 2002, J. Geophys. Res., 107, (A12), 1438
Lin J., Soon W., Baliunas S., 2003, New Astronomy Reviews, 47, 53
Low B., 2001, J. Geophys. Res. 106, 25141
Plunkett S. P., Vourlidas A., Šimberová S., et al. , 2000, SoPh, 194, 371
Priest E. R., Forbes T. G., 2002, A&A Review, 10, 313
Raadu M. A., Mahlherbe J. M., Schmieder B. et al. , 1987, SoPh, 109, 59
Schmieder B., van Driel-Gesztelyi L., Wiik J. et al. , 1997, Proc. of the Fifth SOHO Workshop, ESA SP-404, 663
Wood B. E., Karovska M., Chen J. et al. , 1999, ApJ, 512, 484
Xu A. A., Ding J. P., Ying S. Y., 1984, Acta Astron. Sin., 25, 119
Xuan J. Y., Lin J., 1993, SoPh, 144, 307
Zhong S. H., Gu X. M., Liang H. F., 2004, New Astronomy, 9, No.7, 525 (Paper I)